Nuclear Science and Techniques (2026) 37:27
https://doi.org/10.1007/s41365-025-01850-w

Fast identification of γ-emitting radionuclides based on sequential Bayesian approach

Xuan Zhang[1,2] · **Jian-Wei Huang**[2] · **Lin-Jian Wan**[2,3] · **Jia-Cheng Liu**[4] · **Xiao-Le Zhang**[2] · **De-Hong Li**[2] · **Fei Tuo**[1] · **Zhi-Jun Yang**[2]

Received: 20 August 2024 / Revised: 30 September 2024 / Accepted: 25 November 2024 / Published online: 4 January 2026

Abstract

The rapid identification of γ-emitting radionuclides with low activity levels in public areas is crucial for nuclear safety. However, classical methods rely on full-energy peaks in the integral spectrum, requiring sufficient count accumulation for evaluation, thereby limiting response time. The sequential Bayesian approach, which utilizes prior information and considers both photon energies and interarrival times, can significantly enhance the performance of radionuclides identification. This study proposes a theoretical optimization method for the traditional sequential Bayesian approach. Each photon is processed sequentially, and the corresponding posterior probability is updated in real time using a noninformative prior from the Bayesian theory. By comparing the posterior probabilities of the background and radionuclides based on the energy variance and time interval, the type of γ-rays can be identified (background characteristic γ-rays, Compton plateaus γ-rays, or radionuclide-specific characteristic γ-rays). By integrating the information from these multiple characteristic γ -rays, the presence and type of radionuclides were determined based on the final decision function and a set threshold. Based on theoretical research, verification experiments were conducted using a $LaBr_3$(Ce) detector in both low-and natural background radiation environments with typical radionuclides (^{137}Cs, ^{60}Co, and ^{133}Ba). The results show that this approach can identify ^{137}Cs in 7.9 s and 8.5 s (source dose rate contribution: approximately 6.5×10^{-3} μGy/h), ^{60}Co in 8.1 s and 9.8 s (approximately 4.8×10^{-2} μGy/h), and ^{133}Ba in 4.05 s and 5.99 s (approximately 3.4×10^{-2} μGy/h) under low and natural background radiation, respectively, with a miss rate below 0.01%. This demonstrates the effectiveness of the proposed approach for fast radionuclides identification, even at low activity levels and highlights its potential for enhancing public safety in diverse radiation environments.

Keywords Sequential Bayesian approach · Fast radionuclides identification · $LaBr_3$(Ce) detector · Low background radiation laboratory

1 Introduction

Fast and reliable identification of γ-emitting radionuclides in public areas is crucial for nuclear safety. At customs and security checkpoints, such capabilities help prevent the smuggling of radioactive materials and protect national security. In nuclear power plant monitoring, they support the assessment of environmental and health impacts, enabling rapid decision-making during emergencies to minimize radiation risks. However, low-count detection is challenging due to background noise and heterogeneous media along the transport paths between the sources and detectors, which makes meaningful and timely detection difficult [1–3]. Classical methods used to identify radionuclides involve

---

This work was supported by the Program for NIM-Basic Research Business Expenses Key Field Program, China (No. AKYCX2315).

✉ Fei Tuo
flytuo@163.com

✉ Zhi-Jun Yang
yangzj@nim.ac.cn

[1] National Institute for Radiological Protection, China CDC, Beijing 100088, China

[2] Institute of Ionizing Radiation Metrology, National Institute of Metrology, Beijing 100029, China

[3] State Power Investment Corporation (SPIC) Nucreation Technology Company Ltd., Beijing 100029, China

[4] Nuclear and Radiation Safety Center, Ministry of Ecology and Environment, Beijing 102400, China

analyzing the full-energy peak structure in the spectra, such as the derivative peak searching method [4] and the second derivative peak identification method [5]. Novel detection methods have been proposed to mitigate the impact of noise and environmental backgrounds, including the stochastic resonance method [6], fuzzy logic radioisotopic pattern method [7], Poisson-statistics-based spectral decomposition algorithm [8], and convolutional neural networks (CNNs) [9], etc. Although these methods are reliable, they are limited by their exclusive reliance on the energy information of characteristic γ-rays. Moreover, the effectiveness of data analysis relies heavily on the quality of γ-ray spectral measurements, which requires acquisition of a substantial number of photons to obtain a spectrogram with reliable characteristics. Consequently, these methods cannot meet the urgent need for the real-time detection of radionuclides in public areas and emergency response scenarios.

In 2009, Candy et al. proposed a sequential Bayesian method for radionuclides [3]. This method leverages both the energy characteristic γ-rays and the temporal information of individual photons. The core concept is to process photons individually, to extract all available physical information, discard irrelevant signals from nontarget radionuclides, and retain only those associated with the targeted (threat) radionuclide(s) [10–13]. Candy later extended this approach by incorporating Compton scattering physics, resulting in improved performance over the original photoelectric-only processor [14]. However, studies on the performance and implementation details of this method remain limited. To address this, Xiang Qingpei developed a numerical experimental platform comprising a sequential Bayesian processor and an event sequence generator to validate this technique [15–18]. Using a $\phi 3'' \times 3''$ NaI(Tl) radiation monitoring system, Wen Siying demonstrated that this method provided faster identification and lower detection limits than traditional methods [19]. Wang Changlong enhanced this method by combining pulse characteristics with position transformation, improving the identification of moving targets [20, 21]. Li Zixin improved this by using full-spectrum energy information without relying on temporal information [22]. Wu Zeqian introduced a new model that excludes temporal information but requires extending the number of iterations for the decision-making function to enhance accuracy [23]. Gao Chao proposed a threshold selection method based on Monte Carlo simulations [24]. Li Xiaozhe replaced the background interarrival time distribution assumption from Gaussian to uniform distribution and on this basis, proposed a rapid nuclide recognition system [25–27]. Fang Xinchao further optimized the algorithm by integrating dynamic environmental background parameters and conducting repeated tests to adapt to changes in the environmental background [28]. However, these methods require prior knowledge of sample-specific parameters—such as the time interval variance—which are typically unknown during real-time measurements. Moreover, limited research exists on distinguishing between Compton plateaus, background characteristic γ-rays, and radionuclide-specific characteristic γ-rays. These challenges continue to hinder the practical implementation and reliability of current radionuclide identification techniques.

When instruments are deployed in public spaces, background radiation remains relatively constant regardless of the presence of radionuclides [25]. However, when radionuclides are present, both the energy variance and time intervals between photon events decrease relative to background-only conditions. Furthermore, the distribution characteristics of energy and time within regions of interest (ROIs) differ depending on the type of γ-rays. Leveraging these observations, we propose a theoretically optimized sequential Bayesian approach for rapid identification of γ -emitting radionuclides. Based on the statistical differences between background and radionuclide emissions observed in event mode sequence (EMS), two distinct probabilistic models were developed to characterize their respective behaviors. The posterior probabilities were calculated using Bayes' theorem with noninformative priors and Bayesian factors, while prior probabilities were dynamically updated through sequential detection. By analyzing the relationship between energy- and time-based decision functions and their respective thresholds, the method can effectively differentiate Compton plateaus, background characteristic γ-rays, and radionuclide-specific characteristic γ-rays, etc. Finally, the joint decision function for multiple characteristic γ-rays of the targeted radionuclide is compared with a preset threshold for detecting radionuclides. This model was constructed and validated experimentally using a LaBr$_3$(Ce) detector with typical radionuclides (^{137}Cs, ^{60}Co, and ^{133}Ba) under different background radiation conditions.

2 Method of sequential Bayesian approach

The monoenergetic decomposition concept [3] was proposed to leverage the EMS information. Suppose that the sequence of photons emitted by a radionuclide is a set of photons emitted by several separate monoenergetic sources. More precisely, we define $\xi\left(n;\varepsilon_m(n), \tau_m(n)\right)$, a component of an EMS, as the nth measured photon arrival from the mth monoenergetic source of energy ε_m at arrival time $\tau_m(n)$. The interarrival time is defined as $\Delta\tau_m(n) = \tau_m(n) - \tau_m(n-1)$ with the corresponding set definition of $\Delta\tilde{\tau}_m(n)$. Therefore, the EMS monoenergetic source representation can be written as follows:

$$R(N;\varepsilon, \Delta\tau) := \sum_{m=1}^{M_\varepsilon} \sum_{n=1}^{N_\varepsilon(m)} \xi\left(n;\, \varepsilon_m(n), \Delta\tau_m(n)\right). \tag{1}$$

Considering the effect of the finite detector resolution and other experimental uncertainties, each energy component is approximated as a Gaussian distribution for radionuclides [29].

$$\begin{aligned}&\Pr\left(\varepsilon_m(n) \mid \text{radionuclide}\right) \sim N\left(E_m, \sigma_{E_m}^2\right)\\&= \frac{1}{\sqrt{2\pi}\sigma_{E_m}} \exp\left\{-\frac{\left(\varepsilon_m(n) - E_m\right)^2}{2\sigma_{E_m}^2}\right\}\end{aligned} \tag{2}$$

The energy range of the mth γ-ray was set as the ROI, $\left(\mathrm{ROI}_m\right)$, $\left(E_m - k\sigma_{E_m}, E_m + k\sigma_{E_m}\right)$. k denotes the coverage factor.

$$\begin{aligned}&\Pr\left(\varepsilon_m(n) \mid \text{background or Compton plateau}\right)\\&= p \cdot k_m \cdot \left(\varepsilon_m(n) - E_m\right) + q \cdot \frac{1}{\varepsilon_m^{\text{right}} - \varepsilon_m^{\text{left}}}\\&= p \cdot k_m\left(\varepsilon_m(n) - E_m\right) + q \cdot \frac{1}{\Delta_{E_m}}\end{aligned} \tag{3}$$

where $\varepsilon_m^{\text{left}}$ and $\varepsilon_m^{\text{right}}$ are the left and right energies of ROI_m, respectively; and $\Delta_{E_m} = 2 \cdot k \cdot \sigma_{E_m}$ is the width of the ROI_m region. k_m is the coefficient of the instrument noise interference, $k_m \in \left(-\frac{2}{\Delta_{E_m}^2}, \frac{2}{\Delta_{E_m}^2}\right)$. p and q represent the shares of the Compton plateaus and background, respectively, $p + q = 1$. The interarrival time $\Delta\tau$ is exponentially distributed (based on the Poisson statistics of nuclear decay) such that

$$\begin{aligned}&\Pr\left(\Delta\tau_m(n) \mid \text{radionuclide or background}\right) \sim \mathrm{Exp}\left(\frac{1}{\tau_{m,i}}\right)\\&= \frac{1}{\tau_{m,i}} \cdot e^{-\frac{1}{\tau_{m,i}}\Delta\tau_{m,i}},\end{aligned} \tag{4}$$

the parameter $\tau_{m,i}$ is the mathematical expectation of time interval $\Delta\tau_{m,i}$. When $i = 0$, $\Delta\tau_{m,0}$ represents the time interval for the background of ROI_m and when $i = 1$, $\Delta\tau_{m,1}$ represents the time interval for the radionuclide of ROI_m.

The deviations observed during the comparison between the measured spectrum and expected stable background signal may indicate potential instances of radionuclides. Consequently, a hypothesis test was applied to identify the radionuclides through sequential detection based on the two hypotheses.

H_0 : $R_m(N;\varepsilon, \Delta\tau) \sim \Pr(\varepsilon_m(n), \Delta\tau_m(n) \mid \text{background})$ [if the radionuclide does not exist]

H_1 : $R_m(N;\varepsilon, \Delta\tau) \sim \Pr(\varepsilon_m(n), \Delta\tau_m(n) \mid \text{radionuclide})$ [if the radionuclide exists]

For hypotheses H_0 and H_1, the conditional probability density function $f\left(\varepsilon_m(n) \mid \sigma_{E_m}^2\right)$ of $\varepsilon_m(n)$ can be approximated as follows:

$$H_0 : f_0\left(\varepsilon_m(n) \mid \sigma_0^2\right) = \frac{1}{\Delta_{E_m}}, \; \sigma_0^2 = \frac{\Delta_{E_m}^2}{\left(2 \cdot k_{\mathrm{e}}\right)^2}, \tag{5}$$

$$\begin{aligned}&H_1 : f_1\left(\varepsilon_m(n) \mid \sigma_1^2\right) = \frac{1}{\sqrt{2\pi}\sigma_1} \exp\left\{-\frac{\left(\varepsilon_m(n) - E_m\right)^2}{2\sigma_1^2}\right\},\\&\frac{\Delta_{\varepsilon_m}^2}{\left(2 \cdot k_{\mathrm{c}}\right)^2} \le \sigma_1^2 \le \frac{\Delta_{\varepsilon_m}^2}{\left(2 \cdot k_{\mathrm{e}}\right)^2},\end{aligned} \tag{6}$$

where k_{e} is the coverage factor for a uniform distribution and k_{c} for the corrected Gaussian distribution.

The conditional probability density function $g\left(\Delta\tau_m(n) \mid \frac{1}{\tau}\right)$ of $\Delta\tau_m(n)$ can be described as follows:

$$\begin{aligned}&H_0 : g_0\left(\Delta\tau_m(n) \,\middle|\, \frac{1}{\tau_0}\right) = \frac{1}{\tau_0} \cdot e^{-\frac{\Delta\tau_m(n)}{\tau_0}},\\&\tau_0 = \tau_{\mathrm{bkg}} = \frac{1}{\dot{n}_{\mathrm{bkg}}},\end{aligned} \tag{7}$$

$$\begin{aligned}&H_1 : g_1\left(\Delta\tau_m(n) \,\middle|\, \frac{1}{\tau_1}\right) = \frac{1}{\tau_1} \cdot e^{-\frac{\Delta\tau_m(n)}{\tau_1}},\\&\tau_{\min} \le \tau_1 < \tau_{\mathrm{bkg}},\end{aligned} \tag{8}$$

where τ_0 and τ_1 are the corresponding expected values of $\Delta\tau_m(n)$ under hypotheses H_0 and H_1, respectively; $\dot{n}_{\mathrm{bkg}}$ and τ_{bkg} are the count rates and mean of the sample $\Delta\tau_m(n)$ under the background condition, respectively; $\tau_{\min}$ denotes the parameter that determines the lower limit of detection sensitivity under the alternative hypothesis.

A posterior probability is deduced analytically from a noninformative a priori probability. The prior probability density functions (PDFs) for parameters σ^2 and τ are described as follows:

$$\pi_m\left(\sigma^2\right) = \begin{cases}\pi_{m,0}, & \sigma^2 = \frac{\Delta_{E_m}^2}{(2 \cdot k_{\mathrm{e}})^2}\\ \pi_{m,1}\rho_{m,1}\left(\sigma^2\right), & \frac{\Delta_{E_m}^2}{(2 \cdot k_{\mathrm{c}})^2} \le \sigma^2 < \frac{\Delta_{E_m}^2}{(2 \cdot k_{\mathrm{e}})^2}\end{cases} \tag{9}$$

$$\vartheta_m(\tau) = \begin{cases}\vartheta_{m,0}, & \tau = \tau_{\mathrm{bkg}}\\ \vartheta_{m,1} \cdot h_{m,1}(\tau), & \tau \in \left(\tau_{\min}, \tau_{\mathrm{bkg}}\right)\end{cases} \tag{10}$$

where $\pi_{m,0}, \vartheta_{m,0}$ and $\pi_{m,1}, \vartheta_{m,1}$ are the prior probabilities under hypotheses H_0 and H_1. $\rho_{m,1}\left(\sigma^2\right)$ is the probability density function under H_1 and it holds that $\pi_{m,0} + \pi_{m,1} = 1, \rho_{m,1}\left(\sigma^2\right) \propto \frac{1}{\sigma^2}$. $h_{m,1}(\tau)$ is the probability density function under H_1 and it holds that $\vartheta_{m,0} + \vartheta_{m,1} = 1, h_{m,1}(\tau) \propto \frac{1}{\tau}$.

Bayesian factors are defined as the ratio of the posterior odds to the prior odds [30] and are described as follows:

$$B_m^{\pi}\left(\varepsilon_m(n)\right) = \frac{f_{m,0}\left(\varepsilon_m(n) \mid \sigma^2_{m,0}\right)}{\int \rho_{m,1}\left(\sigma^2_{m,1}\right) f_{m,1}\left(\varepsilon_m(n) \mid \sigma^2_{m,1}\right) \mathrm{d}\sigma^2_{m,1}} \tag{11}$$

$$B_m^{\vartheta}\left(\Delta\tau_m(n)\right) = \frac{g_{m,0}\left(\Delta\tau_m(n) \mid \tau_{m,0}\right)}{\int h_{m,1}\left(\tau_{m,1}\right) \cdot g_{m,1}\left(\Delta\tau_m(n) \mid \tau_{m,1}\right) \mathrm{d}\tau_{m,1}} \tag{12}$$

Subsequently, the posterior probabilities are defined as a function for decision-making:

$$p^{\pi}_{m,0} = \left[1 + \frac{1 - \pi_{m,0}}{\pi_{m,0}} \frac{1}{B_m^{\pi}\left(\varepsilon_m(n)\right)}\right]^{-1} \tag{13}$$

$$p^{\pi}_{m,1} = 1 - p^{\pi}_{m,0} \tag{14}$$

$$p^{\vartheta}_{m,0} = \left[1 + \frac{1 - \vartheta_{m,0}}{\vartheta_{m,0}} \frac{1}{B_m^{\vartheta}\left(\Delta\tau_m(n)\right)}\right]^{-1} \tag{15}$$

$$p^{\vartheta}_{m,1} = 1 - p^{\vartheta}_{m,0} \tag{16}$$

where $p^{\pi}_{m,0}, p^{\vartheta}_{m,0}$ and $p^{\pi}_{m,1}, p^{\vartheta}_{m,1}$ are the posterior probabilities of the energy and time intervals calculated for ROI_m region based on the current radiation under hypotheses H_0 and H_1, respectively. Finally, the current posterior probability is updated to become the prior probability for the next γ-ray, which is foundational for the subsequent ray analysis. The decision making and update of the time interval are subject to the same process.

By combining the decision functions for $\varepsilon_m(n)$ and $\Delta\tau_m(n)$ within the ROI_m region, an assessment regarding the type of γ-rays in ROI_m.

$$\begin{cases} P^{\pi}_{m,0} < P^{\pi}_{m,\mathrm{low\_th}} \,\&\, P^{\vartheta}_{m,0} < P^{\vartheta}_{m,\mathrm{low\_th}} & m\text{th characteristic } \gamma\text{-ray} \\ P^{\pi}_{m,0} > P^{\pi}_{m,\mathrm{up\_th}} \,\&\, P^{\vartheta}_{m,0} > P^{\vartheta}_{m,\mathrm{up\_th}} & \text{Background} \\ P^{\pi}_{m,0} < P^{\pi}_{m,\mathrm{low\_th}} \,\&\, P^{\vartheta}_{m,0} > P^{\vartheta}_{m,\mathrm{up\_th}} & \text{A characteristic } \gamma\text{-ray from background} \\ P^{\pi}_{m,0} > P^{\pi}_{m,\mathrm{up\_th}} \,\&\, P^{\vartheta}_{m,0} < P^{\vartheta}_{m,\mathrm{low\_th}} & \text{Compton plateau from other high-energy rays} \\ \text{otherwise} & \text{Continue} \end{cases} \tag{17}$$

where $P^{\pi}_{i,\mathrm{up\_th}}$ and $P^{\pi}_{i,\mathrm{low\_th}}$ represent the upper and lower thresholds of the energy decision function, respectively, and $P^{\vartheta}_{i,\mathrm{up\_th}}$ and $P^{\vartheta}_{i,\mathrm{low\_th}}$ denote the upper and lower thresholds of the time decision function, respectively. The thresholds are specified in terms of false alarm (α) and miss (β) rates as follows.

$$p^{\pi,\vartheta}_{m,\mathrm{up\_th}} = \frac{1 - \alpha^{\pi,\vartheta}}{1 - \alpha^{\pi,\vartheta} + \beta^{\pi,\vartheta}} \tag{18}$$

$$p^{\pi,\vartheta}_{m,\mathrm{low\_th}} = \frac{\alpha^{\pi,\vartheta}}{1 - \beta^{\pi,\vartheta} + \alpha^{\pi,\vartheta}} \tag{19}$$

The joint decision function for a radionuclide is defined in Eq. (20):

$$p_X = \sum_m \lambda_m \cdot p^{\pi}_{m,0} \cdot p^{\vartheta}_{m,0} \tag{20}$$

$$\lambda_m = \frac{\eta_m \cdot \kappa_m}{\sum_N \eta_N \cdot \kappa_N} \tag{21}$$

where p_X denotes the decision function for the radionuclide and λ_m denotes the weight coefficient of the corresponding γ-ray. η_m and κ_m represent the branching ratio and the intrinsic detection efficiency of γ-rays, respectively. N is the total number of γ-rays of radionuclide I_X.

$$\begin{cases} P_X < P_{X,\mathrm{low\_th}} & \text{Radionuclide exists} \\ P_{X,\mathrm{low\_th}} \le P_X \le P_{X,\mathrm{up\_th}} & \text{Continue} \\ P_{X,\mathrm{up\_th}} < P_X & \text{Radionuclide does not exist} \end{cases} \tag{22}$$

where $P_{X,\mathrm{up\_th}}$ and $P_{X,\mathrm{low\_th}}$ are the upper and lower thresholds, respectively.

3 Experimental designs

3.1 Experimental conditions and equipment

A proof-of-concept experiment was developed to assess the feasibility of the sequential Bayesian processor and its ability to detect and identify targeted radionuclides. This experiment was conducted in the low-background radiation laboratory at the Nuclear and Radiation Safety Center's Changyang Base (NRSC) and Natural Background Radiation Laboratory at the National Institute of Metrology's Changping Base (NIM). The radiation levels in the low background radiation laboratory ($\dot{n}_{\mathrm{low\_bkg}} = 59.3\ \mathrm{s}^{-1}$, $H^{*}(10)_{\mathrm{low}} = 12.6\,\mathrm{nSv/h}$) were significantly lower than the natural background radiation levels ($\dot{n}_{\mathrm{nor\_bkg}} = 165.9\ \mathrm{s}^{-1}$, $H^{*}(10)_{\mathrm{nor}} = 111\ \mathrm{nSv/h}$). The experimental setup is shown in Fig.1 along with the equipment used consisting of source, measurement instrument including a $\mathrm{LaBr_3(Ce)}$ detector listed in Table 1. The radionuclide source was positioned centrally in direct line

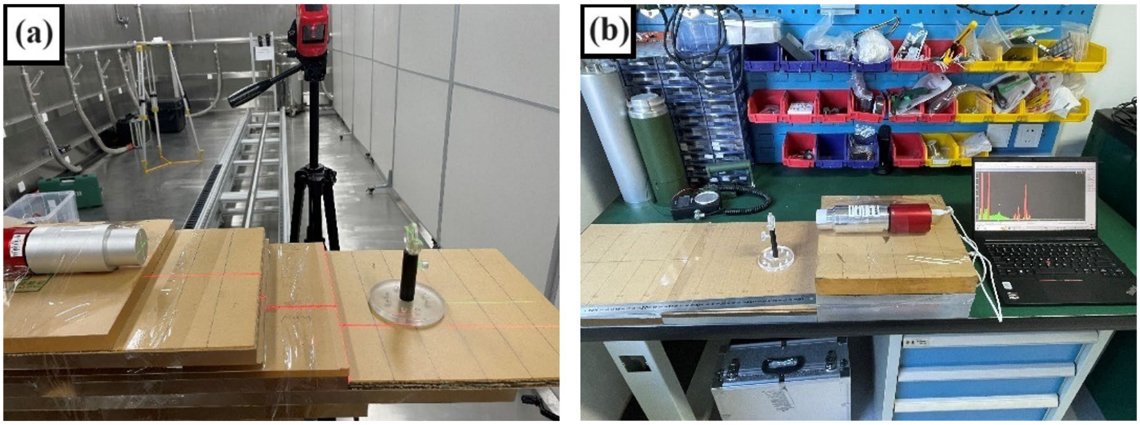

Fig. 1 (Color online) Experimental setup. **a** Low background radiation laboratory. **b** Natural background radiation laboratory

Table 1 Experimental equipment and source information

Type	Activity	Manuf ID	γ-rays energy (keV)	γ-rays branch (%)	γ-rays FWHM (keV)
^{137}Cs	8.92×10^{3} Bq@19/3/23	341 NIM	661.62	85.01	18.36
^{60}Co	3.50×10^{4} Bq@17/3/23	191101	1173.23	99.85	23.87
		NIM	1332.50	99.98	26.09
^{133}Ba	1.34×10^{5} Bq@22/3/23	0609-9	79.6+ 81.0[a]	2.63 + 33.31	7.31
			276.40	7.13	11.87
			302.85	18.31	12.64
			356.01	62.05	13.57
		NIM	383.85	8.94	13.97
LaBr$_3$(Ce) (1.5″×1.5″)	–	SAINT-GOBAIN	–	–	–
ADC	–	10870017 Jiechuang Nuclear Instrument (Beijing) Technology Co., Ltd	–	–	–

[a] The γ-ray energies of 79.6 keV and 81.0 keV from ^{133}Ba are too close to be resolved by the LaBr$_3$(Ce) detector. As a result, these two energies have been combined and analyzed as a ROI

with the LaBr$_3$(Ce) detector face at distances varying from 7 to 52 cm, with increments of 5 cm in each case. The source dose rate contributions were calculated based on the distance between the source and detector, activity of the source, and other relevant parameters [31, 32], as shown in Table 2. The parameters of eight monoenergetic γ-rays emitted by three targeted radionuclides, ^{137}Cs, ^{60}Co, and ^{133}Ba, were obtained from the radionuclide database, as shown in Table 1.

3.2 Parameter preset

A sequential Bayesian processor was embedded within a radionuclide library comprising 22 radionuclides. The parameters of radionuclides for ^{137}Cs, ^{60}Co, and ^{133}Ba are listed in Table 1. The ROIs were set to full width at tenth maximum (FWTM) interval, where the coverage factor was $k = 2.146$. The background count rates within each ROIs were determined using a continuous 12-hour measurement of the environmental background.

Because of the unbiasedness of the prior probability, the initial value of the prior probability was set to 0.5. For any feasible radionuclide identification method, the following performance criteria are generally required: when no radionuclide is present, the false alarm rate is not significant, and a high detection performance is not required. However, when a radionuclide is present, the miss rate, detection time, and sample size should be minimized. Therefore, in this study, the parameters are set to $\alpha = 0.2$ and $\beta = 0.2$.

Table 2 Source dose rate contribution at different distances

Distance (cm)	Source dose rate contribution (μGy·h^{-1})					
	^{137}Cs		^{60}Co		^{133}Ba	
	Low[a]	Natural[b]	Low[a]	Natural[b]	Low[a]	Natural[b]
7	0.13	0.13	2.07	1.88	1.82	1.70
12	4.5×10^{-2}	4.4×10^{-2}	0.72	0.66	0.63	0.59
17	2.3×10^{-2}	2.2×10^{-2}	0.36	0.33	0.32	0.30
22	1.4×10^{-2}	1.3×10^{-2}	0.22	0.19	0.19	0.18
27	9.1×10^{-3}	8.9×10^{-3}	0.14	0.13	0.13	0.12
32	6.5×10^{-3}	6.4×10^{-3}	0.10	9.0×10^{-2}	9.1×10^{-2}	8.5×10^{-2}
37	4.9×10^{-3}	4.8×10^{-3}	7.7×10^{-2}	6.8×10^{-2}	6.8×10^{-2}	6.4×10^{-2}
42	–	–	6.0×10^{-2}	5.3×10^{-2}	5.3×10^{-2}	4.9×10^{-2}
47	–	–	4.8×10^{-2}	4.2×10^{-2}	4.2×10^{-2}	4.0×10^{-2}
52	–	–	3.9×10^{-2}	3.4×10^{-2}	3.4×10^{-2}	3.2×10^{-2}

[a] The "low" data are calculated based on the activity levels of the source as recorded in March 2023

[b] The "natural" data are calculated based on the activity levels of the source as recorded on March 2024

4 Results and discussions

4.1 Background experiment

4.1.1 Results of pulse-height spectra and EMS progress

Using a fast radionuclide identification method, the typical radionuclides (^{137}Cs, ^{60}Co, and ^{133}Ba) were detected under conditions of low and natural background radiation. The pulse-height spectra (PHS) and EMS detected under low and natural background radiation are shown in Fig. 2a–d. In the spectra and EMS, we first observe a low-energy peak centered at approximately 35.5 keV, which is an intrinsic characteristic γ-rays in LaBr$_3$(Ce). This is attributed to the sum of 95.6% of the 31.83 keV K$_\alpha$ X-ray response and 90% of the 5.6 keV Auger electron response in the EC decay process, by referring to the theoretical calculation [33]. Subsequently, we observe a β continuum with an end point of 263 keV mixed with the Compton continua, primarily from the 788.7 and 1435.8 keV of ^{138}La and the 1460.8 keV of ^{40}K. With increasing energy, the 788.7 keV bump is shown to extend to higher energies and end at approximately 1 MeV. This is because of the coincidence of the 788.7 keV γ with the β^- continuum [33]. Finally, we observed the 1436 keV gamma, but it was displaced to a higher energy by approximately 37 keV to 1473 keV owing to the coincident capture of X-rays, resulting in Ba K-level filling following K-electron capture. Similarly, the hump near 1441 keV on the low-energy side of the 1473 line is a result of the 1436 keV gamma plus 5 keV owing to the 1436 keV gamma plus 5 keV because of the coincident capture of X-rays when the Ba L-level fills following L-electron capture [34]. A comparison of the PHS and EMS between low- and natural-background radiation revealed a higher abundance of low-energy photons in the natural background. Furthermore, the significant presence of 1460 keV γ-rays from ^{40}K in the natural background radiation contributed to the overlap of the peaks, making it difficult to distinguish between the 1436 keV and 1473 keV peaks.

According to Eqs. (13)–(17), the sequential Bayesian method was used to detect background characteristic γ-rays. As shown in Fig. 3a–c, although both the energy and time decision functions exhibit oscillations in the early stages of identification, however, they do not affect their overall trends or final identification result. Under low background radiation, a 35.5 keV γ-ray could be identified within 0.764 s, whereas under natural background radiation, it could be detected within 0.572 s. The higher presence of low-energy photons in natural background radiation makes it more challenging to make evaluations based on the energy decision function than on the time decision function, as illustrated in Fig. 3a. The 1473 keV γ-ray can be identified under low background radiation with a detection time of 6.83 s, under natural background radiation identification encounters difficulties owing to interference from the 1460 keV γ-ray. Nevertheless, by combining 1436 keV and 1473 keV γ-rays into a single ROI, rapid identification becomes possible with a detection time of 2.77 s. Additionally, under low background radiation, the identification speed is slower because of the non-Gaussian distribution, as illustrated in Fig. 2a, with a detection time of 13.67 s.

As each photon is processed, the decision function is sequentially updated until one of the thresholds (target/non-target) is crossed, indicating a threat or non-threat. As shown in Fig. 4a–c, the decision function gradually increases as events are processed until it exceeds the high threshold, indicating the absence of radionuclides at 57.85 s, 113.58 s, and 15.73 s for ^{137}Cs, ^{60}Co, and

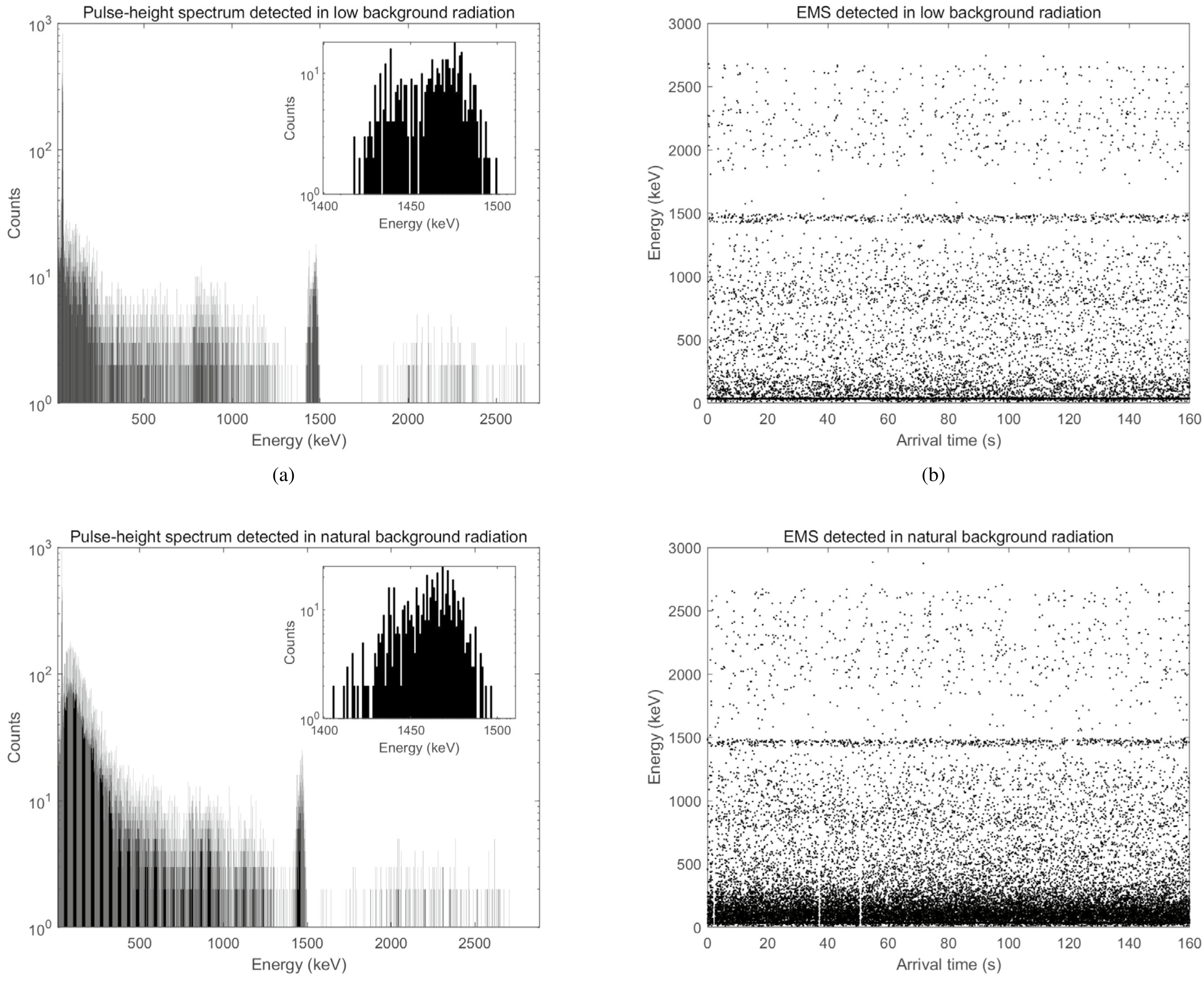

(a) (b) (c) (d)

Fig. 2 Pulse-height spectra and EMS of background particle events in 160 s. **a** Pulse-height spectra under low background radiation. **b** EMS under low background radiation. **c** Pulse-height spectra under natural background radiation. **d** EMS under natural background radiation

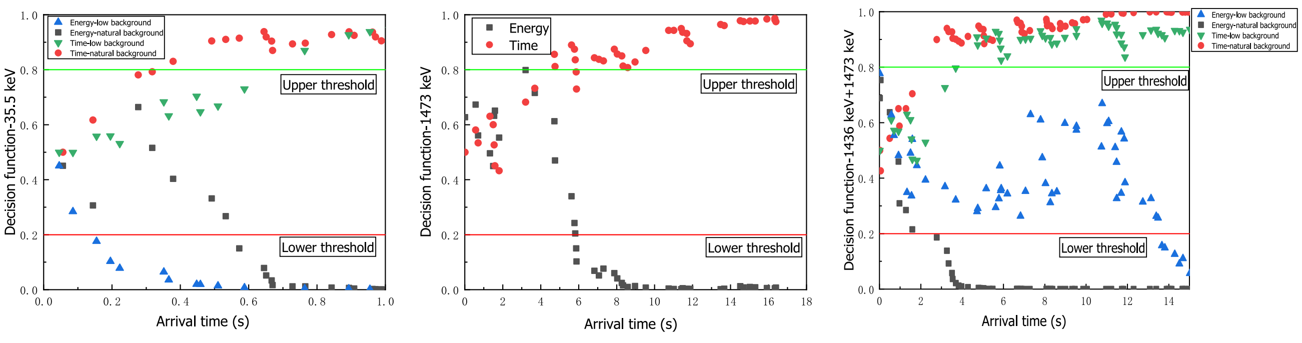

(a) (b) (c)

Fig. 3 Decision functions for different ROIs under different background radiation. **a** Decision function for the ROI at 35.5 keV (detection times: 0.764 s under low background, 0.572 s under natural background). **b** Decision function for the ROI at 1473 keV (detection time: 6.83 s under low background). (c) Decision function for the ROI at 1436 keV+1473 keV (detection times: 13.67 s under low background, 2.77 s under natural background)

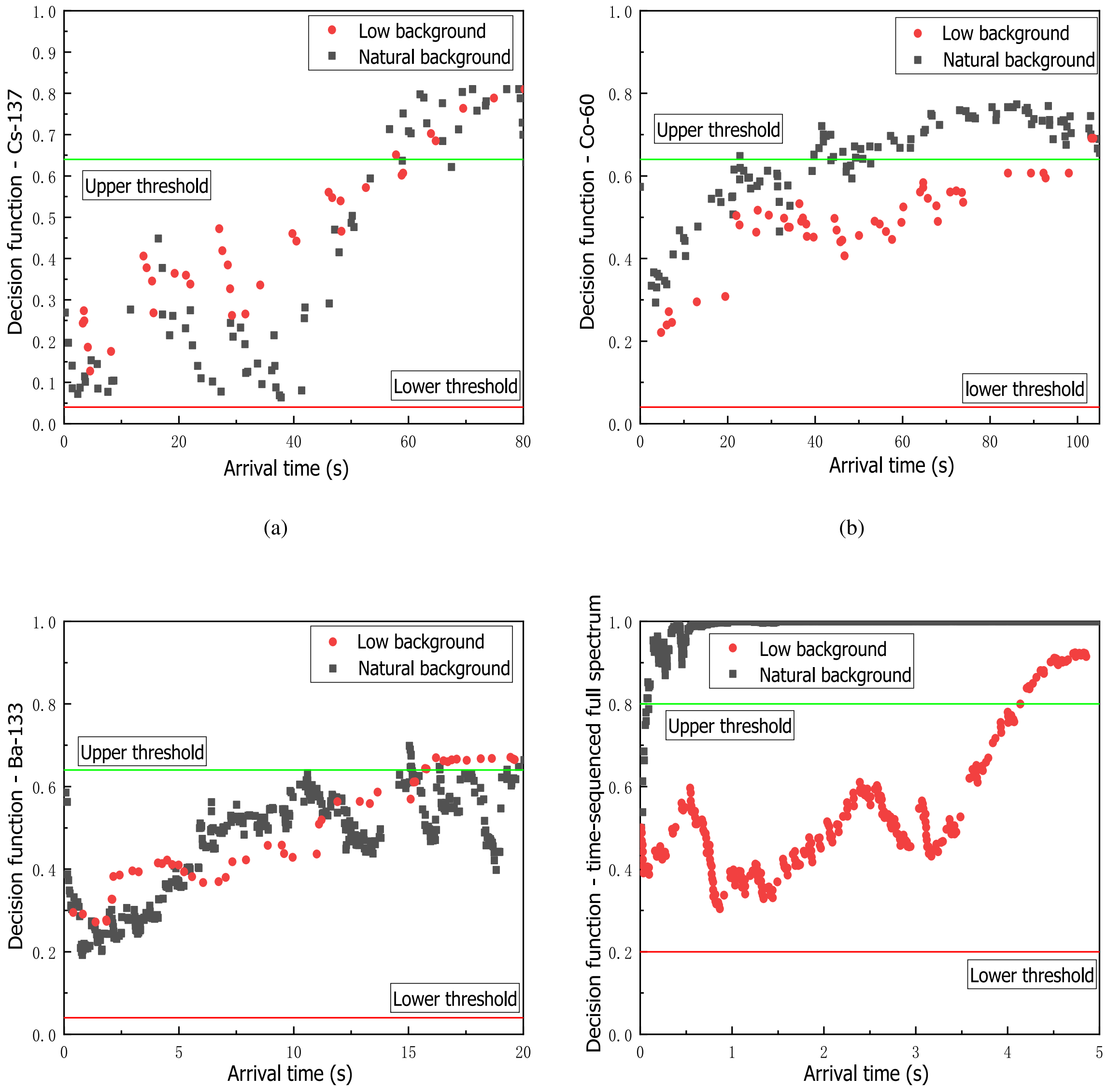

(a)

(b)

(c)

(d)

Fig. 4 Decision functions for targeted radionuclides under different background radiation. **a** Decision function for ^{137}Cs (detection times: 57.85 s under low background, 56.72 s under natural background). **b** Decision function for ^{60}Co (detection times: 113.58 s under low background, 22.82 s under natural background). **c** Decision function for ^{133}Ba (detection times: 15.73 s under low background, 15.05 s under natural background). (d) Decision function for time-sequenced full spectrum (detection times: 4.14 s under low background, 0.074 s under natural background)

^{133}Ba under low background radiation, and at 56.72 s, 22.82 s and 15.05 s under natural background radiation, respectively. The corresponding numbers of γ-rays within the ROI were 28, 60, and 38 under low background radiation and 52, 24, and 288 under natural background radiation. As shown in Fig. 4c, the decision function for ^{133}Ba oscillates more under natural background due to the higher number of low-energy photons, without affecting the overall trend. In contrast, the ROIs for ^{137}Cs and ^{60}Co were at higher energy levels, resulting in fewer oscillations than ^{133}Ba.

This identification was achieved using the energy and time interval information of the ROI. However, by disregarding information from individual ROIs and considering only the temporal characteristics of the full spectrum, a hypothesis can be formulated [35]. By computing the posterior probability using only a time-sequential Bayesian approach for decision-making based on the full spectrum, a faster identification speed was achieved, as shown in Fig. 4d. The detection time did not exceed 5 s. Therefore, for background discrimination, the sequential Bayesian decision-making method based on the time-sequenced full spectrum was more effective. This method be used initially to determine the presence of background.

4.1.2 Detection performance experiments

To evaluate the detection performance of the proposed method, a series of experiments were conducted under both low and natural background radiation without radionuclides, with 20 repeated detection experiments for each condition. The analysis was based on the decision functions for ^{137}Cs, ^{60}Co, ^{133}Ba and a time-sequenced full spectrum. Table 3 presents the average detection time, average number of γ-rays per ROI, and false-alarm rate for different radionuclides.

Based on the time-sequenced full-spectrum radionuclide detection method [35], the false alarm rates under low and natural background radiation were 15% and 30%, respectively, which indicates the probability of misidentifying non-source events as source events. The false identification rate of ^{137}Cs under natural background radiation was 5%. False-alarm events often result in increased detection times and larger sample sizes. These false alarm events were primarily concentrated in the early stages of detection, as shown in Fig. 5a. During the initial phase, the limited sample size led to significant statistical fluctuations in the data, which amplified the influence of random errors and resulted in false-alarm events. In particular, as shown in Fig. 5b, most energy samples fall near the center of the ROI, and the random fluctuations in the timing of radiation samples cause the decision function to mistakenly indicate the presence of a radionuclide. The impact of these random errors diminished as the sample size gradually

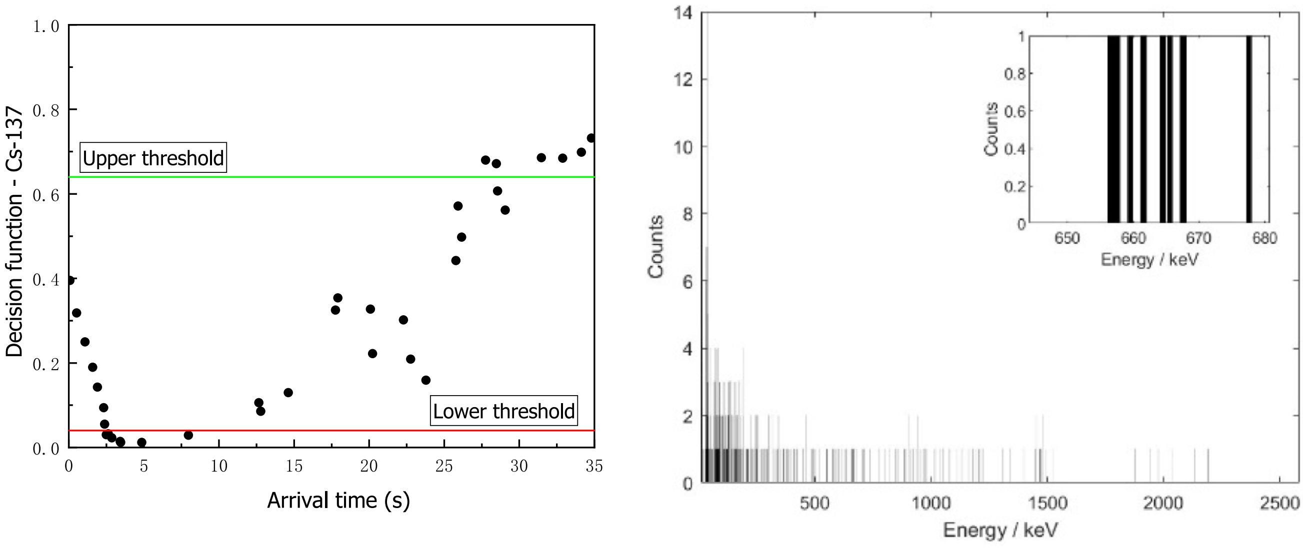

(a)

(b)

Fig. 5 Decision function and pulse-height spectrum of ^{137}Cs under natural background radiation. **a** Decision function (detection time: 27.76 s). **b** Pulse-height spectrum (at false detection time: 2.51 s)

Table 3 The results of 20 experiments for each of the three radionuclides and time-sequenced full spectrum under low and natural background radiation

Radionuclide	^{137}Cs		^{60}Co		^{133}Ba		Time-sequenced full spectrum	
	Low	Natural	Low	Natural	Low	Natural	Low	Natural
Average detection time (s)	53.43±53.12	30.16±26.06	246.43±178.63	89.87±93.68	72.0±59.62	16.51±14.77	5.29±6.22	4.48±4.69
Average number of γ-rays per ROI	25±30	29±30	73±55	48±57	49±43	64±61	310±366[a]	659±744[a]
t value	−3.30		1.369		−0.942		−1.88	
P value	0.743		0.179		0.352		0.071	
False alarm rate (%)	0	5	0	0	0	0	15	30

[a] The number of γ-rays was based on the total energy range of γ-rays

increased, reducing the occurrence of false alarms and ultimately achieving accurate background identification.

Using an independent samples two-sided *t*-test to compare the number of γ-rays for background identification under various background radiation, the results in Table 3 indicated that the difference between the two conditions was not statistically significant ($P > 0.05$). This suggests that, statistically, the required number of γ-rays for background identification is similar under a natural background and low background radiation.

This finding explains the relatively short time required for background identification under natural background irradiation. This is because regardless of the specific radionuclide, the number of γ-ray detections required for background discrimination remains consistent. However, the count rate under natural background radiation exceeded that under low-background conditions. Consequently, background identification was accomplished more rapidly using natural background radiation.

4.2 Radionuclide detection experiment

4.2.1 Results of pulse-height spectra and EMS progress

^{137}Cs was positioned 37 cm in front of the LaBr$_3$(Ce) detector with a source dose rate contribution of 4.9 nGy/h. ^{60}Co and ^{133}Ba were placed 52 cm from the LaBr$_3$(Ce) detector with source dose-rate contributions of 3.9×10^{-2} μGy/h and 3.4×10^{-2} μGy/h, respectively, under low background radiation. However, under natural background radiation, the source dose rate contributions were 4.8 nGy/h for ^{137}Cs, 3.4×10^{-2} μGy/h for ^{60}Co, and 3.2×10^{-2} μGy/h for ^{133}Ba. The decision functions are shown in Fig. 6.

Radionuclide identification was conducted under known background conditions, and the initial probability was adjusted accordingly. As each photon is discriminated and processed, the decision function is sequentially updated until one of the thresholds is crossed, signifying non-threat (upper threshold) or threat (lower threshold). Based on the time-sequenced full spectrum radionuclides detection method [35], the detection times for the presence of radionuclides are 9.99 s and 1.91 s for ^{137}Cs, 2.49 s and 1.29 s for ^{60}Co, and 0.43 s and 0.29 s for ^{133}Ba, under low and natural background radiation, respectively. The corresponding numbers of γ rays were 640 and 370 for ^{137}Cs, 183 and 265 for ^{60}Co, and 67 and 94 for ^{133}Ba.

The identification times for ^{137}Cs, ^{60}Co, and ^{133}Ba under low background radiation are 5.01 s, 9.49 s, and 3.43 s, with corresponding numbers of γ-rays per ROI of 15, 16, and 30, respectively. Under natural background radiation, the identification times are 8.19 s, 12.33 s, and 5.50 s, with corresponding numbers of γ-rays per ROI of 22, 23, and 70, respectively. Figure 7 illustrates the pulse-height spectra at the time of detection. At the moment of detection, only a small number of counts had accumulated in the ROI for ^{137}Cs, ^{60}Co, and ^{133}Ba, resulting in an indistinct or unformed peak.

Using the time-sequenced full spectrum method to determine the presence or absence of a nuclide is faster than using the ROI, except for ^{137}Cs under low background radiation. Therefore, first use the sequential Bayesian method based on a time-sequenced full spectrum to determine the presence of radionuclides and then use ROI-based analysis to identify the specific radionuclides.

When exposed to a ^{60}Co source, decision functions for ROIs at various energy levels were calculated. The analysis revealed that the ROI at 35.5 keV was identified as a background characteristic γ-ray at 0.497 s and 0.683 s, the ROI at 661.62 keV was recognized as a Compton plateau at 28.0 and 40.59 s, and the ROI at 1332.5 keV was classified as a characteristic γ-ray at 7.41 s and 8.68 s under low and natural background radiation, respectively, as shown in Fig. 8. These results demonstrate that simultaneously applying the time interval and energy decision functions effectively discriminates between Compton plateaus, background characteristic γ-rays, and radionuclide-specific characteristic γ-rays.

4.2.2 Detection performance experiments

Experiments were conducted by varying the distance between the source and detector to evaluate the performance of the proposed method. The radionuclides were placed at different distances in front of the LaBr$_3$(Ce) detector, and the measurements were repeated 20 times. The average detection time was calculated and plotted for each experimental group, as shown in Fig. 9. All measurements successfully detected the corresponding radionuclides, yielding a miss rate of 0% for the background detection. Overall, the miss rate remained below 0.01%.

When the detection distance is set to 7 cm (source dose rate contribution: 0.13 μGy/h, refer to Table 2), the ^{137}Cs detection time is 0.36 s and 0.49 s under low and natural background radiation, respectively. The distance increased along with the detection time. When the distance reaches 32 cm, the average detection time increases to 7.9 s and 8.5 s. For ^{60}Co, the average detection time is within 2.0 s when the detection distance is within 22 cm. At a distance of 47 cm, the average detection time is 8.1 s and 9.8 s under low and natural background radiation, respectively. For ^{133}Ba, as the distance increased from 2 to 52 cm, the detection time under low background conditions increased from 0.062 s to 4.05 s, whereas under natural background radiation, it increased from 0.058 s to 5.99 s, meeting the requirements for rapid identification.

The relationship between the source dose rate contribution and detection time, as depicted in Fig. 9a, demonstrates

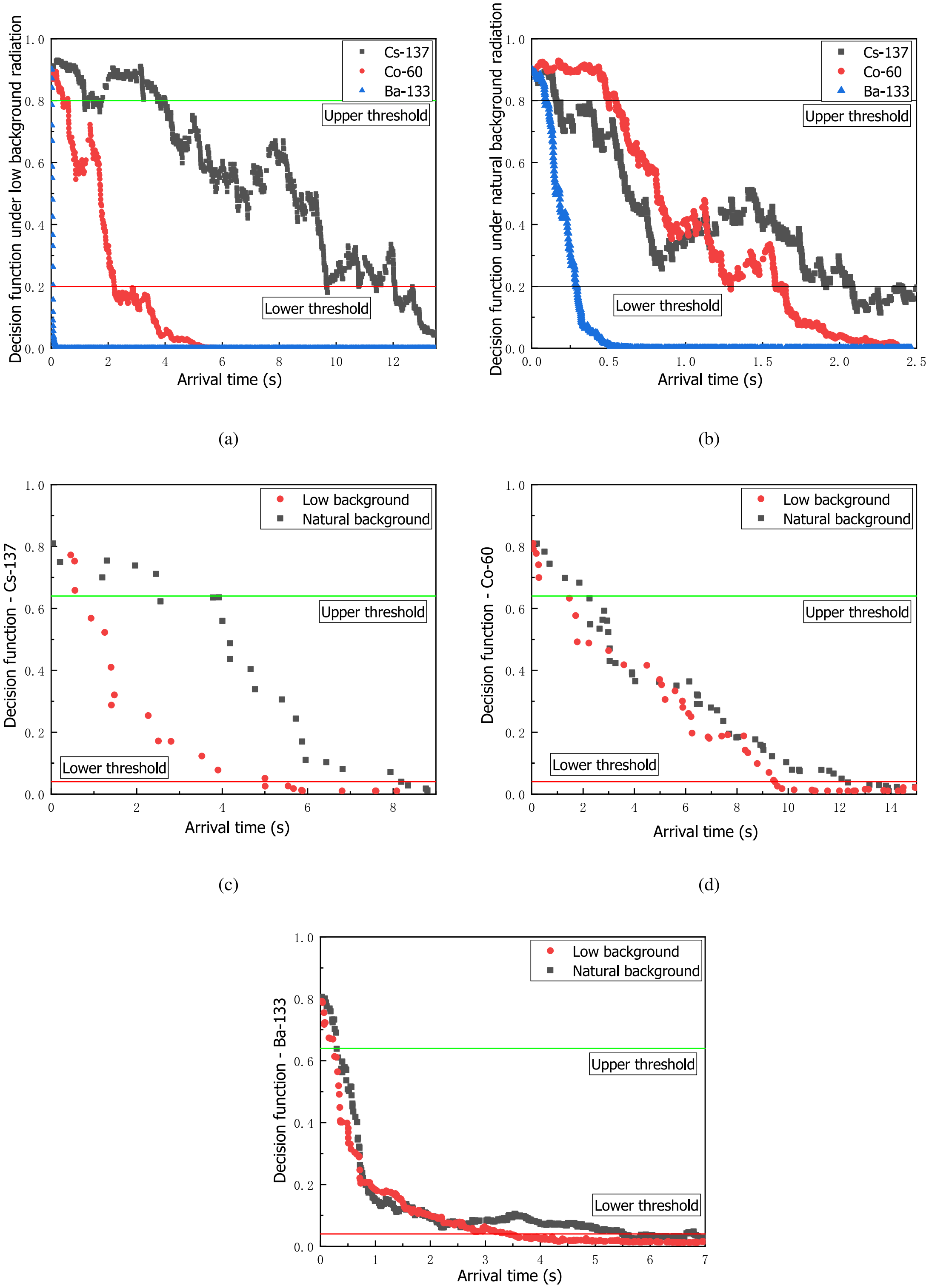

(a)

(b)

(c)

(d)

(e)

Fig. 6 Decision functions under different background radiation. **a** Decision function for time-sequenced full spectrum under low background radiation (detection times: ^{137}Cs—9.99 s, ^{60}Co—2.49 s, ^{133}Ba—0.43 s). **b** Decision function for time-sequenced full spectrum under natural background radiation (detection times: ^{137}Cs—1.91 s, ^{60}Co—1.29 s, ^{133}Ba—0.29 s). **c** Decision function for ^{137}Cs (detection times: 5.01 s under low background, 8.19 s under natural background). **d** Decision function for ^{60}Co (detection times: 9.49 s under low background, 12.33 s under natural background). **e** Decision function for ^{133}Ba (detection times: 3.43 s under low background, 5.50 s under natural background)

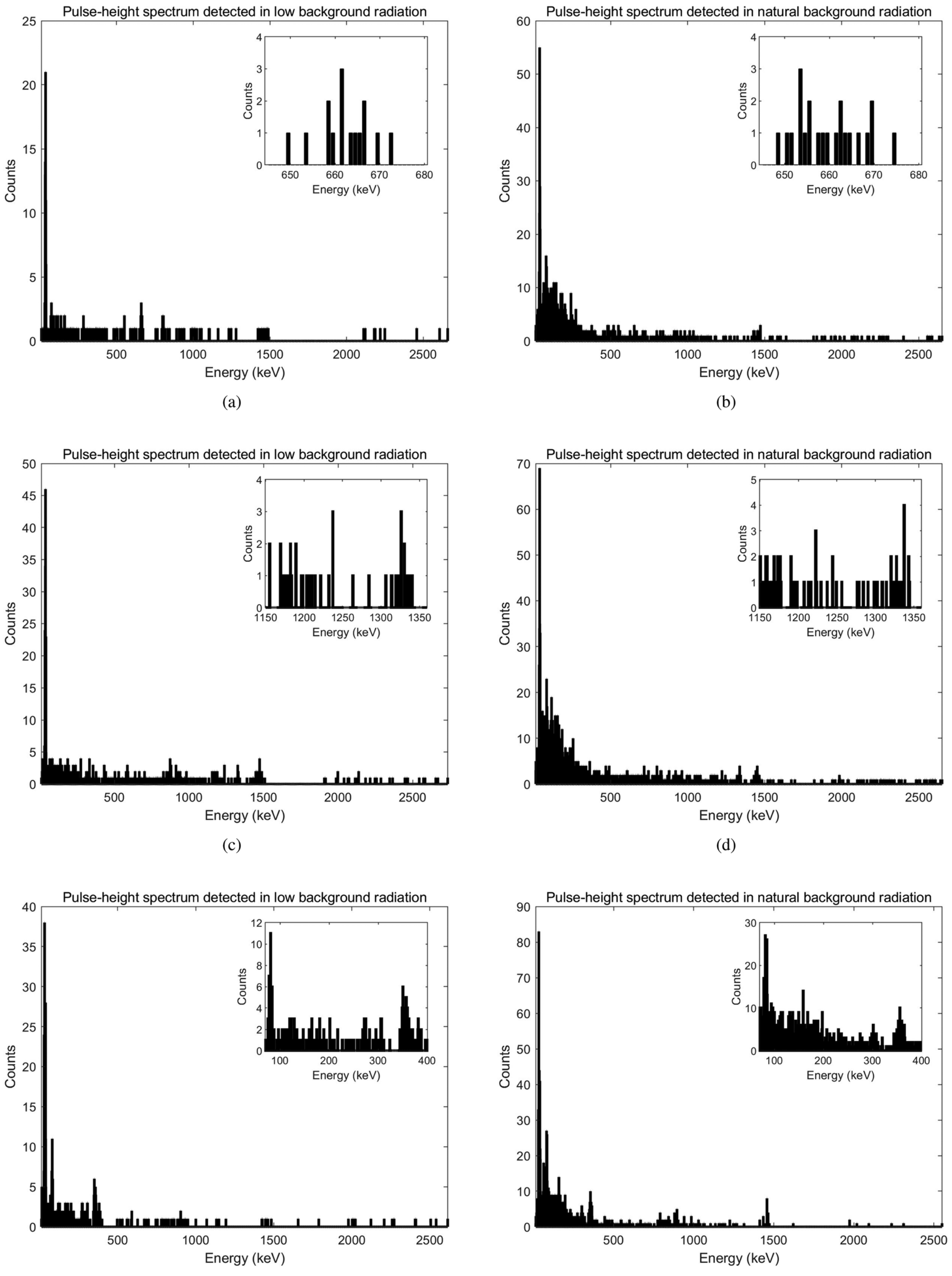

(a)

(b)

(c)

(d)

(e)

(f)

Fig. 7 Pulse-height spectra for targeted radionuclides at sequential Bayesian when first detected under different background radiation. **a** Pulse-height spectrum for ^{137}Cs under low background radiation. **b** Pulse-height spectrum for ^{137}Cs under natural background radiation. **c** Pulse-height spectrum for ^{60}Co under low background radiation. **d** Pulse-height spectrum for ^{60}Co under natural background radiation. **e** Pulse-height spectrum for ^{133}Ba under low background radiation. **f** Pulse-height spectrum for ^{133}Ba under natural background radiation

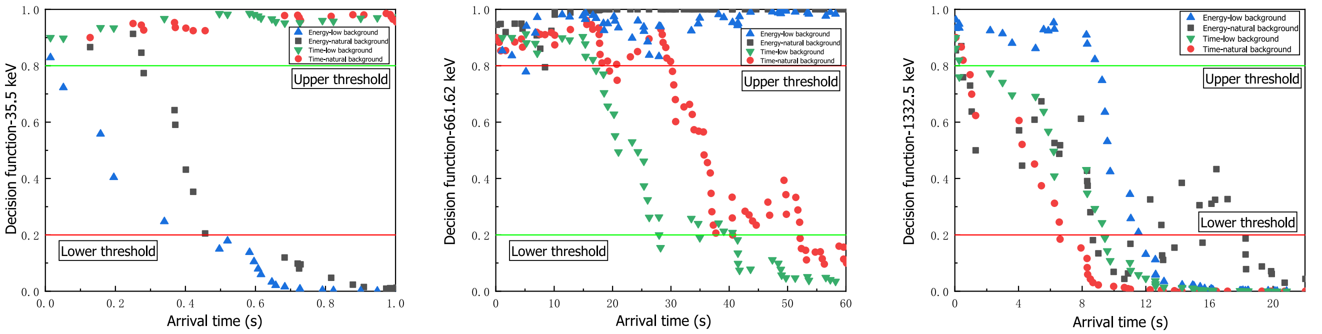

(a)

(b)

(c)

Fig. 8 Decision functions for different ROIs in the presence of ^{60}Co under different background radiation. **a** Decision function for the ROI at 35.5 keV (detection times: 0.497 s under low background, 0.683 s under natural background). **b** Decision function for the ROI at 661.62 keV (detection times: 28.0 s under low background, 40.59 s under natural background). **c** Decision function for the ROI at 1332.5 keV (detection times: 7.41 s under low background, 8.68 s under natural background)

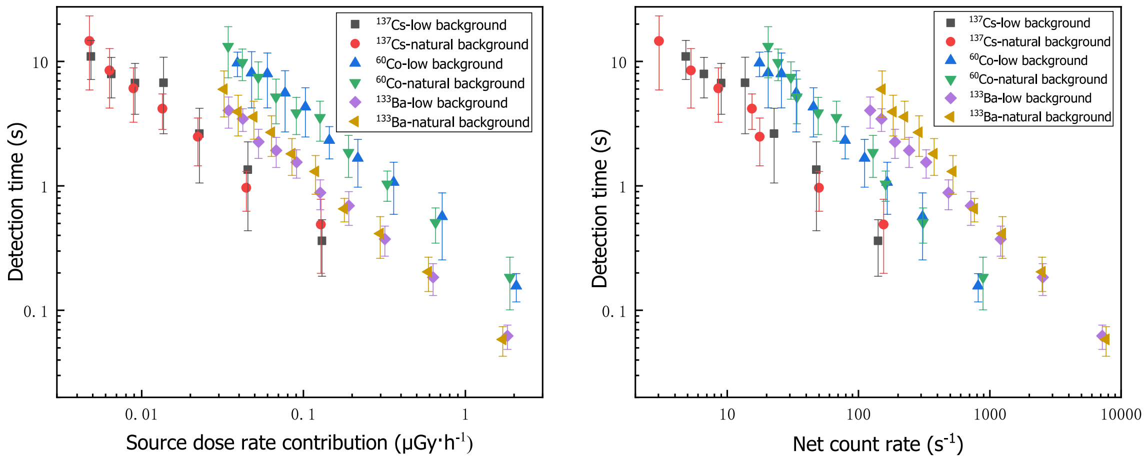

(a)

(b)

Fig. 9 Relationships between detection time, source dose rate contribution, and net count rate. **a** Relationship between detection time and source dose rate contribution. **b** Relationship between detection time and net count rate

a power-law relationship, meaning detection time decreases as dose rate increases. The detection times remained largely consistent across different background radiation levels, indicating that the radionuclide identification performance was affected to a lesser extent by variations in the background radiation. The relationship between net count rate and detection time followed the same pattern, as shown in Fig. 9b. However, under equivalent net count rate conditions, the detection times followed the order ^{133}Ba > ^{60}Co >^{137}Cs. Similarly, at the same source dose-rate contribution, ^{60}Co exhibited longer detection times than ^{133}Ba and ^{137}Cs. This disparity arises because ^{60}Co emits two high-energy characteristic γ-rays, whereas ^{133}Ba emits multiple γ-rays. Consequently, ^{133}Ba achieved a higher net count rate than ^{60}Co for the same source dose-rate contribution.

5 Conclusions and prospects

This study proposes a fast identification approach for γ-emitting radionuclides in public areas based on a sequential Bayesian approach. This method assumes that the energy variance and time intervals decrease when radionuclides are present compared with the background. Two distinct probability models were developed: one for the background radiation and the other for the target radionuclide. The posterior probability is obtained using noninformative prior and a Bayesian factor based on the different characteristics of the energy and time interval distributions. The target radionuclide is identified by integrating the decision functions of multiple characteristic γ-rays.

This approach leverages the differing energy and time distributions of γ-rays within regions of interest (ROIs). By analyzing the relationship between the energy and time decision functions and their corresponding thresholds, the method effectively distinguishes between Compton plateaus, background characteristic γ-rays, and radionuclide-specific characteristic γ-rays—a capability rarely reported in other sequential Bayesian approaches. In addition, unlike traditional methods, which require preset values for the mean and variance of the time interval when a radionuclide is present, this approach requires only a preset time range that is smaller than the background time interval. This innovation helps avoid the influence of unpredictable factors such as source activity, thereby enhancing its applicability across different conditions.

A particular realization of the process was successfully developed and applied to proof-of-concept experimental data demonstrating its overall feasibility under low and natural background radiation. This approach can identify ^{137}Cs in 7.9 s and 8.5 s (source dose rate contribution: approximately 6.5×10^{-3} μGy/h), ^{60}Co in 8.1 s and 9.8 s (approximately 4.8×10^{-2} μGy/h), and ^{133}Ba in 4.05 s and 5.99 s (approximately 3.4×10^{-2} μGy/h,) under low and natural background radiation, respectively, with a miss rate of less than 0.01%. This demonstrates the effectiveness of the proposed method for the rapid identification of radionuclides, even at low activity levels, which can help establish an accurate and timely radioactive material detection system as an additional nuclear safety application option, particularly for public safety.

To fully explore the applicability of this method across various scenarios, experiments were conducted under both low background radiation simulation conditions in which the detector is shielded in systems such as item monitoring [36], and natural background radiation simulation conditions in which the detector is directly exposed to the environment. Without radionuclides, background detection occurs more quickly under natural background radiation than under low background radiation because, although the number of particles required is the same, a higher dose rate accelerates the process. In the presence of radionuclides, the detection times remained largely consistent across the different background radiation levels.

However, this approach requires prolonged evaluation time for background discrimination. Therefore, we recommended first using the sequential Bayesian method based on a time-sequenced full spectrum to determine the presence of radionuclides [35] and then use ROI-based analysis to identify the specific radionuclides.

Future work will focus on further optimizing the algorithm. To enhance its applicability in complex environments, research efforts should aim at achieving rapid detection and identification of radionuclide types in mixed compositions, particularly under challenging background conditions and dynamic source movements.

Author contributions All authors contributed to the study conception and design. Material preparation, data collection and analysis were performed by Xuan Zhang, Jian-Wei Huang, Lin-Jian Wan and Fei Tuo. The first draft of the manuscript was written by Xuan Zhang and all authors commented on previous versions of the manuscript. All authors read and approved the final manuscript.

Data availability The data that support the findings of this study are openly available in Science Data Bank at https://cstr.cn/31253.11.sciencedb.j00186.00772 and https://www.doi.org/10.57760/sciencedb.j00186.00772.

Declarations

Conflict of interest The authors declare that they have no conflict of interest.

References

1. C.J. Sullivan, S.E. Garner, M. Lombardi et al., Evaluation of key detector parameters for isotope identification. 2007 IEEE Nuclear Science Symposium Conference Record. **2**, 1181–1184 (2007). https://doi.org/10.1109/NSSMIC.2007.4437217
2. N. Carron, *An Introduction to the Passage of Energetic Particles Through Matter* (CRC Press, Boca Raton, 2007), p.384. https://doi.org/10.1201/9781420012378
3. J.V. Candy, E. Breitfeller, B.L. Guidry et al., Physics-based detection of radioactive contraband: a sequential Bayesian approach. IEEE T. Nucl. Sci. **56**, 3694–3711 (2009). https://doi.org/10.1109/TNS.2009.2034374
4. W.F. Chen, Development of measurement and analysis software for multi-channel gamma-ray spectrometer. Master's dissertation, China University of Geosciences (2011)
5. M.A. Mariscotti, A method for automatic identification of peaks in the presence of background and its application to spectrum analysis. Nucl. Instrum. Methods **50**, 309–320 (1967). https://doi.org/10.1016/0029-554X(67)90058-4
6. J.M. Zhang, Methods and experiments for weak nuclear signal detection and nuclide identification. Dissertation, University of Science and Technology of China (2017)
7. M. Alamaniotis, J. Young, L.H. Tsoukalas, Assessment of fuzzy logic radioisotopic pattern identifier on gamma-ray signals with application to security. Int. J. Monit. Surveillance Technol. Res. **2**, 1–21 (2014). https://doi.org/10.4018/ijmstr.2014010101
8. K. Nagata, Y.I. Mototake, R. Muraoka et al., Bayesian spectral deconvolution based on Poisson distribution: Bayesian measurement and virtual measurement analytics (VMA). J. Phys. Soc. Jpn. **88**, 044003 (2019). https://doi.org/10.7566/JPSJ.88.044003
9. G. Daniel, F. Ceraudo, O. Limousin et al., Automatic and real-time identification of radionuclides in Gamma-Ray spectra: a new method based on convolutional neural network trained with synthetic data set. IEEE T. Nucl. Sci. **67**, 644–653 (2020). https://doi.org/10.1109/TNS.2020.2969703
10. J.V. Candy, E. Breitfeller, B. Guidry et al., Radioactive contraband detection: a Bayesian approach. OCEANS **2009**, 1–10 (2009). https://doi.org/10.23919/OCEANS.2009.5422451
11. J.V. Candy, K. Sale, B.L. Guidry et al., Bayesian processing for the detection of radioactive contraband from uncertain measurements.

In: 2nd IEEE International Workshop on Computational Advances in Multi-Sensor Adaptive Processing. 49–52 (2007). https://doi.org/10.1109/CAMSAP.2007.4497962
12. J.V. Candy, *Bayesian Signal Processing: Classical, Modern and Particle Filtering Method* (Wiley, Hoboken, 2016)
13. J.V. Candy, E. Breitfeller, B.L. Guidry et al., Physics-based detection of radioactive contraband: a sequential Bayesian approach. IEEE T. Nucl. Sci. **56**, 3694–3711 (2009). https://doi.org/10.1109/TNS.2009.2034374
14. J.V. Candy, D.H. Chambers, E.F. Breitfeller et al., Threat detection of radioactive contraband incorporating compton scattering physics: a model-Based processing approach. IEEE T. Nucl. Sci. **58**, 214–230 (2011). https://doi.org/10.1109/TNS.2010.2090361
15. Q.P. Xiang, D.F. Tian, F.H. Hao et al., Off-line experiments on radionuclide detection based on the sequential Bayesian approach. Nucl. Instrum. Meth. Phys. Res. Sect. **729**, 212–219 (2013). https://doi.org/10.1016/j.nima.2013.07.046
16. Q.P. Xiang, D.F. Tian, J.Y. Zhu et al., Numerical study on the sequential Bayesian approach for radioactive materials detection. Nucl. Instrum. Meth. Phys. Res. Sect. **697**, 107–113 (2013). https://doi.org/10.1016/j.nima.2012.09.031
17. Q.P. Xiang, Z.H. Wang, D.F. Tian et al., On-line experiments on rapid detection of radionuclides based on sequential Bayesian analysis. J. Radioanal. Nucl. Chem. **306**, 57–70 (2015). https://doi.org/10.1007/s10967-015-4072-y
18. Q.P. Xiang, Research on nuclide identification algorithm based on sequential Bayesian method, Dissertation, China Academy of Engineering Physics (2014)
19. S.Y. Wen, B.R. Wang, G. Xiao et al., The study on nuclide identification algorithm based on sequential Bayesian analysis. Nucl. Eng. Dete. Tech. **36**, 179–183 (2016). https://doi.org/10.3969/j.issn.0258-0934.2016.02.015
20. C.L. Wang, J.M. Zhang, Rapid detection of weak radionuclide in moving target. Inf. Tec. Net. Sec. **37**, 137–139 (2018). https://doi.org/10.19358/j.issn.2096-5133.2018.03.033
21. C.L. Wang, The study of radioactive nuclide identification method based on random pulse information and Bayesian classifier. Master dissertation, Southwest University of Science and Technology (2018)
22. Z.X. Li, J.R. Cang, J.F. Zhu et al., Fast nuclide identification based on energy weight graph. Nucl. Electron. Detect. Technol. **39**, 501–507 (2019). https://doi.org/10.3969/j.issn.0258-0934.2019.04.022
23. Z.Q. Wu, B.R. Wang, J. Sun, Design of radionuclides identification algorithm based on sequence Bayesian method. IOP Conf. Ser. Mater. Sci. Eng **569**, 052047 (2019). https://doi.org/10.1088/1757-899X/569/5/052047
24. C. Gao, Z.L. Fang, Q.L. Wen et al., Study on sequential Bayesian radionuclide identification approach: threshold and detection capability. 2019 IEEE 3rd Information Technology, Networking, Electronic and Automation Control Conference. pp. 469–473 (2019). https://doi.org/10.1109/ITNEC.2019.8729225
25. X.Z. Li, Q.X. Zhang, H.Y. Tan et al., Fast nuclide identification based on a sequential Bayesian method. Nucl. Sci. Tech. **33**, 29 (2022). https://doi.org/10.1007/s41365-021-00982-z
26. X.Z. Li, Q.X. Zhang, H.Y. Tan et al., Research of nuclide identification method based on background comparison method. Appl. Radiat. Isot. **192**, 110596 (2023). https://doi.org/10.1016/j.apradiso.2022.110596
27. X. Li, C. Dong, Q. Zhang et al., Research and design of a rapid nuclide recognition system. J. Instrum. **17**, T06008 (2022). https://doi.org/10.1088/1748-0221/17/06/T06008
28. X.C. Fang, J. Wu, Y. Yuan et al., Study on the sequential Bayesian approach for a CsI(Tl)-based radioactive material detection system. Nucl. Instrum Meth. Phys. Res. A **1038**, 166894 (2022). https://doi.org/10.1016/j.nima.2022.166894
29. E. Rohee, R. Coulon, F. Carrel et al., Benchmark of the non-parametric Bayesian deconvolution method implemented in the SINBAD code for X/γ rays spectra processing. Nucl. Instrum. Meth. Phys. Res. A **836**, 91–97 (2016). https://doi.org/10.1016/j.nima.2016.08.025
30. J.V. Candy, Model-based signal processing. J. Acoustical Soc. Am. **119**, 2553 (2006). https://doi.org/10.1121/1.2184129
31. M.M. Ninkovic, J.J. Raicevic, F. Adrovic, Air kerma rate constants for gamma emitters used most often in practice. Radiat. Prot. Dosim. **115**, 247–250 (2005). https://doi.org/10.1093/rpd/nci131
32. M.M. Ninkovic, F. Adrovic, Air kerma rate constants for nuclides important to gamma ray dosimetry and practical application. Med. Phys. (2012). https://doi.org/10.5772/39170
33. F.G.A. Quarati, I.V. Khodyuk, C.W.E. Eijk et al., Study of ^{138}La radioactive decays using LaBr$_3$ scintillators. Nucl. Instrum. Meth. Phys. Res. A **683**, 46–52 (2012). https://doi.org/10.1016/j.nima.2012.04.066
34. C. Hao, B.H. Sun, L.H. Zhu et al., Intrinsic background radiation of LaBr$_3$(Ce) detector via coincidence measurements and simulations. Nucl. Sci. Tech. **31**, 99 (2020). https://doi.org/10.1007/s41365-020-00812-8
35. L.J. Wan, X. Zhang, C.L. Zhang et al., Research of fast detection method for radionuclides based on sequential Bayesian approach. Nucl. Tech. (in Chinese) **48**, 010404 (2025). https://doi.org/10.11889/j.0253-3219.2025.hjs.48.240190
36. K. Ishii, Belt-conveyor type non-destructive radioactive caesium contamination monitoring machine. Radioisotopes **67**, 67–73 (2018). https://doi.org/10.3769/radioisotopes.67.67